Int. J. Electrochem. Sci., 13 **(2018)** 11405 – 11417, doi: 10.20964/2018.12.38

International Journal of
ELECTROCHEMICAL
SCIENCE
www.electrochemsci.org

Hollow Structured $LiFePO_4$ /C Microspheres in situ Prepared by a One-Pot Template-Free Method as Cathode for Lithium-Ion Batteries

Yuan Jin,, Haiyan Wang and Xincun Tang**

Hunan Provincial Key Laboratory of Chemical Power Sources, Hunan Provincial Key Laboratory of Efficient and Clean Utilization of Manganese Resources, College of Chemistry and Chemical Engineering, Central South University, Changsha 410083, P. R. China
*E-mail: wanghy419@csu.edu.cn (H.Wang); tangxincun@163.com (X.Tang)

Received: 31 July 2018 / *Accepted:* 29 September 2018 / *Published:* 5 November 2018

The effective control of the nanostructure is recognized as an effective method for improving the electrochemical performance of the $LiFePO_4$ cathode; nevertheless, it is still a great challenge to simultaneously achieve high tap density and excellent electrochemical performance. Herein, we develop a hydrothermal method combined with a sintering process to synthesize monodispersed $LiFePO_4$/C microspheres with an open channel interior. The microsphere assembled of ultrathin nanosheets shows a unique hollow structure with open channel which endows the hollow $LiFePO_4$/C with a good balance of high specific surface area (28.9 $m^2 g^{-1}$) and tap density (1.2 g cm^{-3}), revealing prospect of the promising application. This sample with 2.6 wt% in-situ carbon coating exhibits a superior reversible capacity. At high current densities of 5 and 10 C, discharge capacities of 115 and 93.5 mAh g^{-1} could be obtained, respectively, indicating excellent rate performance of the as-prepared hollow $LiFePO_4$/C sample. The superior lithium storage performance should originate from the accelerated charge transfer and Li-ion diffusion from the unique hierarchical hollow microsphere structure, as well as from the improved electronic conductivity ascribed from the in-situ carbon coating. This work highlights that the structure-based design is an effective approach to achieve superior lithium storage performance together with high tap density for $LiFePO_4$ cathode material.

Keywords: Open hollow channel; High tap density; Superior lithium storage performance; Lithium ion batteries.

1. INTRODUCTION

Structure designing has been considered as a promising method for constructing advanced functional materials.[1, 2] In particular, three-dimensional micro-nano hierarchical structures with

specific morphologies composed of nanosized anisotropic structures have attracted substantially attention in recent years.[2-4] It is anticipated that the hierarchical structures would inherit both of the superiorities of the nanoscale building blocks and the secondary architectures. These features always endow hierarchically nanostructured materials with versatile composition, large specific surface area, and high mechanical and thermal stability, which make it attractive in many applications fields, including solar cells, Li-ion batteries and supercapacitors.[5-8]

Recently, hollow materials have attracted more attention in chemistry and material fields on account of their low density, versatile composition, large specific surface area, mechanical separator stability and thermal stability, and the penetrability of the surface.[9-13] However, its low electrical conductivity ($\sim 10^{-9}$ S cm^{-1}) and inferior Li^+ diffusion ($\sim 1.8\times10^{-14}$ cm^2 s^{-1}) dramatically restrict its application in Li-ion batteries. Different synthesis methods such as templating, self-assembly, galvanic replacement, and hydrothermal methods have recently been reported for the preparation of a desirable shell structure with an interior void space.[8, 14-17] Among these methods, hydrothermal method is believed to be a universal and straightforward approach for the control of morphology and size with high uniformity.[18, 19] $LiFePO_4$ with different structures have been synthesized to overcome the kinetic limitation by virtues of shortened Li^+ ion diffusion distance and increased surface area. Although, the lithium storage performance has been promoted to some extent through the morphology designing, however, most of them still suffer from poor rate capability and severe cycling instability.[20-22] In our previous work, three-dimensional nanoplates assembled $LiFePO_4$ microspheres were synthesized by a facial straightforward solvothermal method, whose tap density was up to 1.4 g cm^{-3}.[23] Unfortunately, the as-prepared $LiFePO_4$ microspheres showed relatively low surface area and poor penetration of electrolyte, thus leading to inferior lithium storage performance. It has been proved that 3D hierarchical hollow structures with robust secondary architectures can effectively prevent structural degradation upon cycling, benefit electrolyte penetration and Li^+ ion diffusion, thus leading to satisfactory discharge capacity and cycling stability of active materials. Moreover, the electronic conductivity of $LiFePO_4$ could be highly improved through conductive carbon coating, which would facilitate charge transfer at high rates, ensuring better rate performance.[24-26] From the above discussion, designing $LiFePO_4$ with unique 3D hierarchical hollow structures combined with surface carbon coating would be an effective approach to improve its lithium storage performance.

In this work, we developed a straightforward synthetic route to prepare 3D hierarchical hollow structured $LiFePO_4$/C microsphere. This unique structure consists of open hollow interior and functional shell assembled of ultrathin nanosheet. The formation of this unique 3D hierarchical hollow structure has been investigated to follow an asymmetric Ostwald ripening mechanism. The unique structure gives rise to the good balance of high surface area and high tap intensity for the powder, leading to shortened Li-ion diffusion length and better electrolyte penetration. Moreover, the in-situ carbon coating layer could result in significantly enhanced electronic conductivity. Owing to the combined merits above, the as-prepared 3D hierarchical hollow structured $LiFePO_4$/C sample exhibits high discharge capacity, excellent cycling stability and superior rate capability.

2. EXPERIMENTAL SECTION

2.1. Synthesis of hollow $LiFePO_4$/C

In a typical synthesis condition, raw materials, LiH_2PO_4 (10 mmol), $FeSO_4 \cdot 7H_2O$ (10 mmol) and citric acid (0.5 mmol) were added into 40 mL polyethylene glycol (PEG) in a round-bottom flask with continuous magnetic stirring at a constant temperature of 80 °C in an oil bath pot. After stirring for 40 min, the obtained light grey solution was moved into a 50 mL Teflon vessel, sealed, and then heated at 200 °C for 8 h. The obtained precursor was gathered by filtration, and rinsed thoroughly with distilled water and absolute ethanol. As follows, the precipitate was dried at 80 °C for 48 h in vacuum and heated at 700 °C for 6 h in Ar/H_2 (5 vol% H_2) flow. For comparison, intermediate samples formed at different reaction times were also synthesized. The experimental details of pure LFP or micro-nano $LiFePO_4$/C are shown in the author's previous paper.[23]

2.2 Materials characterization

The crystalline structure of the final products was examined by X-ray powder diffraction (XRD, Rigaku Ulyima IV, Japan) using graphite-monochromatized CuKα radiation. The composition and valence of the material element for the final products was examined by X-ray photoelectron spectroscopy (XPS, DX-2700). The structure and morphology were characterized using field-emission scanning electron microscopy (SEM, Zeiss ULTRA 55) and high-resolution transmission electron microscopy (HRTEM, JEOL, Japan) with an acceleration voltage of 200 KV. The Raman spectrum was collected by a Labram-010 laser Raman spectrometer. The tap density was calculated by the measured volume of the packed powder and mass. The specific surface area was carried out by means of the Brunauer-Emmett-Teller (BET) equation on account of the nitrogen adsorption isotherm received with a Micromeritics Gemini VII apparatus (Surface Area and Porosity Analyzer).

2.3 Cell fabrication and electrochemical measurements

Electrochemical performance of the obtained hollow $LiFePO_4$/C composite material was evaluated by CR2016 coin cells. The cathode electrode was made by the mixture of active material ($LiFePO_4$), acetylene black and poly-vinylidence fluoride (80:10:10 wt %). Galvanostatic charged and discharge tests were evaluated from 0.1 C to 10 C (1C=170 mA g^{-1}) with a Land 2001 battery test system. Cyclic voltammetry (CV) and Electrochemical impedance spectroscopy (EIS) was performed by—Zahner elektrik (IM6ex).

3. RESULTS AND DISCUSSION

The crystal structure and phase purity of the as-prepared hollow $LiFePO_4$/C was detected by XRD and the structure refinement was also carried out. As shown in Fig. 1, all the diffraction peaks in

the XRD pattern well matched with the orthorhombic olivine-type structure $LiFePO_4$ (JCPDS card no 81-1173) without any impurity, suggesting the high purity of the hollow $LiFePO_4$/C. Based on the refined results, the crystal parameters of the as-prepared hollow $LiFePO_4$ /C were calculated to be a=10.318 Å，b=6.002 Å, c=4.691 Å. Also, good crystallization of $LiFePO_4$ could be seen from the sharp diffraction peeks.

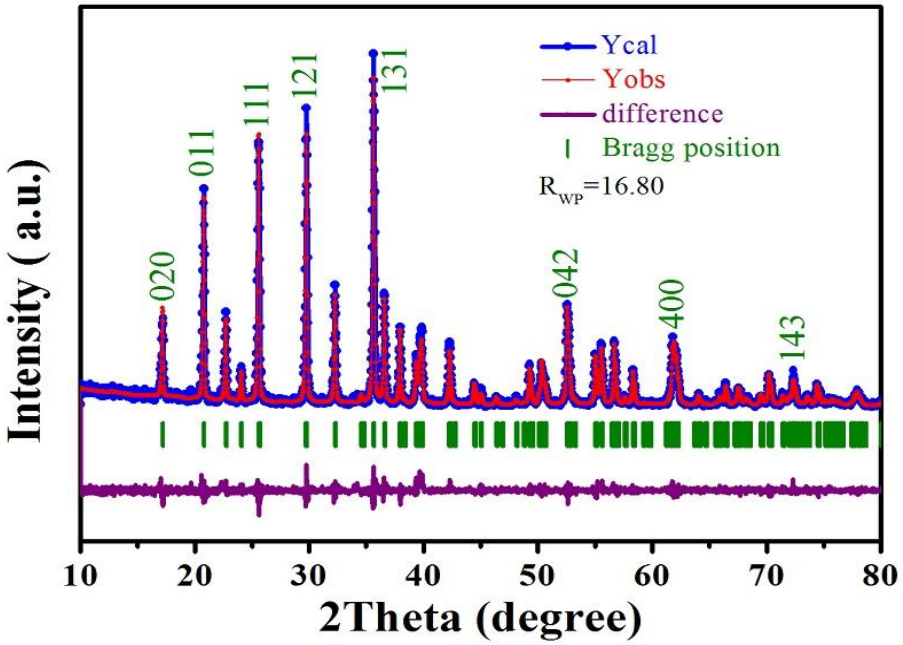

Figure 1. XRD pattern of the as-prepared hollow $LiFePO_4$/C

The morphology of the hollow $LiFePO_4$/C precursor was investigated by SEM and TEM. As shown in Fig. 2a-b, mono-dispersed hollow microspheres with an open channel can be observed clearly. This hollow microsphere shows an average diameter of about 0.5~1 μm. Interestingly, the magnified SEM image shows that these microspheres are assembled from 2D nanosheets. The morphology of the 3D hierarchical hollow structured $LiFePO_4$/C microspheres was further tested by high-resolution TEM. The hollow interior microstructure of the synthesized $LiFePO_4$/C is well demonstrated in Fig. 2c-e.

The cross section (Fig. 2c) and longitudinal section (Fig. 2d, e) of the synthesized hollow LiFePO4/C show an open channel throught the microsphere. The open cahnnel is benefical for the deep penetration of electrolyte, which means that the special structure could afford plenty of space for the effective contact of electrolyte and dramatically shortened the diffusion diatance of Li^+. As seen from the Fig. 2f-g, the hollow $LiFePO_4$/C is assembled by nanosheets with several dozens of nanometers, which is consistent with the SEM image. A hollow interior runs through the whole microsphere. [27] Besides, this hierarchical nanosheets-assembled microsphere with the open channel could effectively reduce the volume change during the charge-discharge process and increase the reaction sites for Li-ion storage.[19, 28] The clear lattice fringes in Fig. 2g demonstrate the high crystallinity of the hollow $LiFePO_4$/C. Element mapping images (Fig. 2h-k) demonstrate well distribution of Fe, P and O elements among the microsphere.

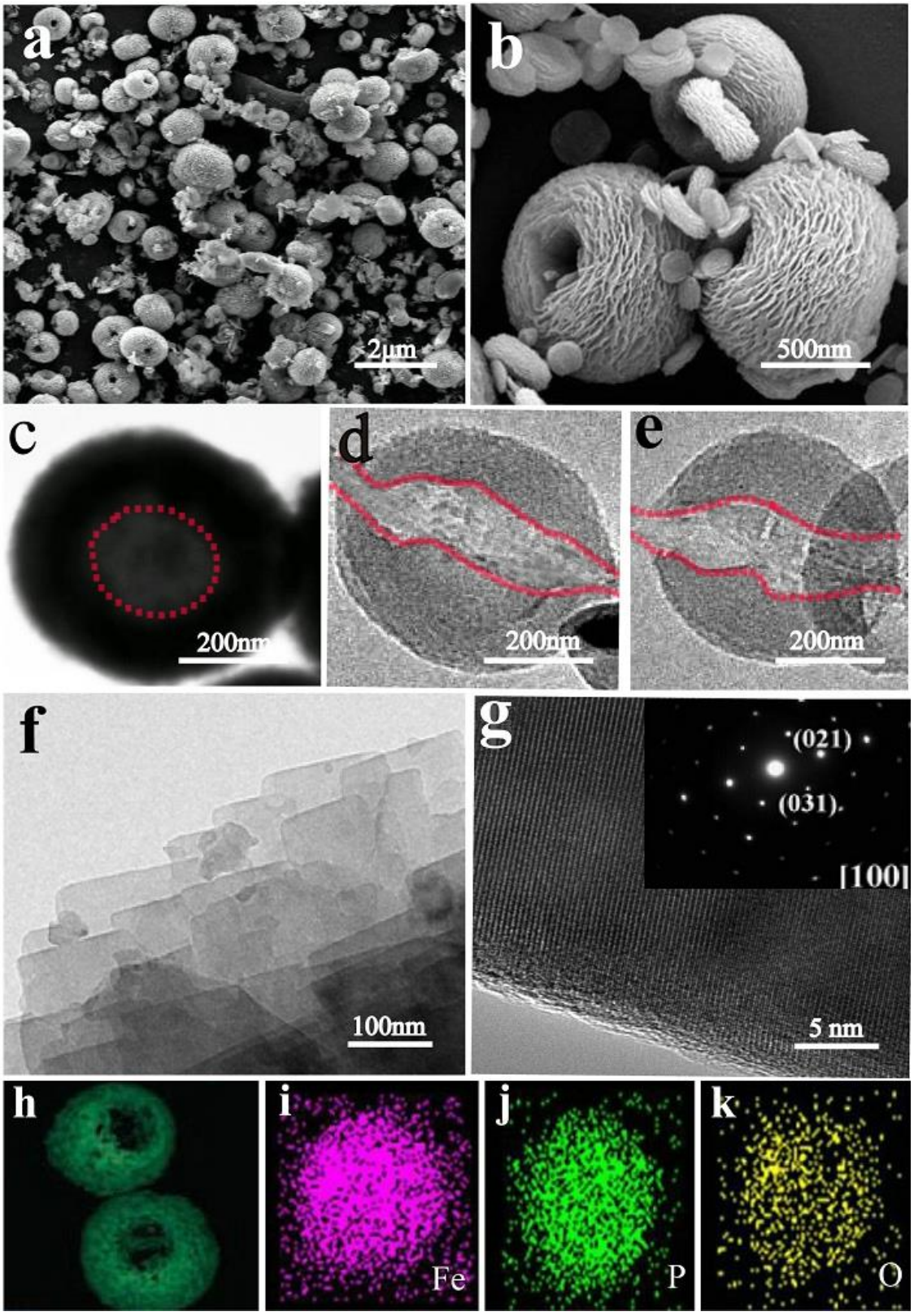

Figure 2. Microstructure of the hollow $LiFePO_4$/C: (a, b) FE-SEM images; (c-g) HRTEM images; (h-k) Elemental mapping images.

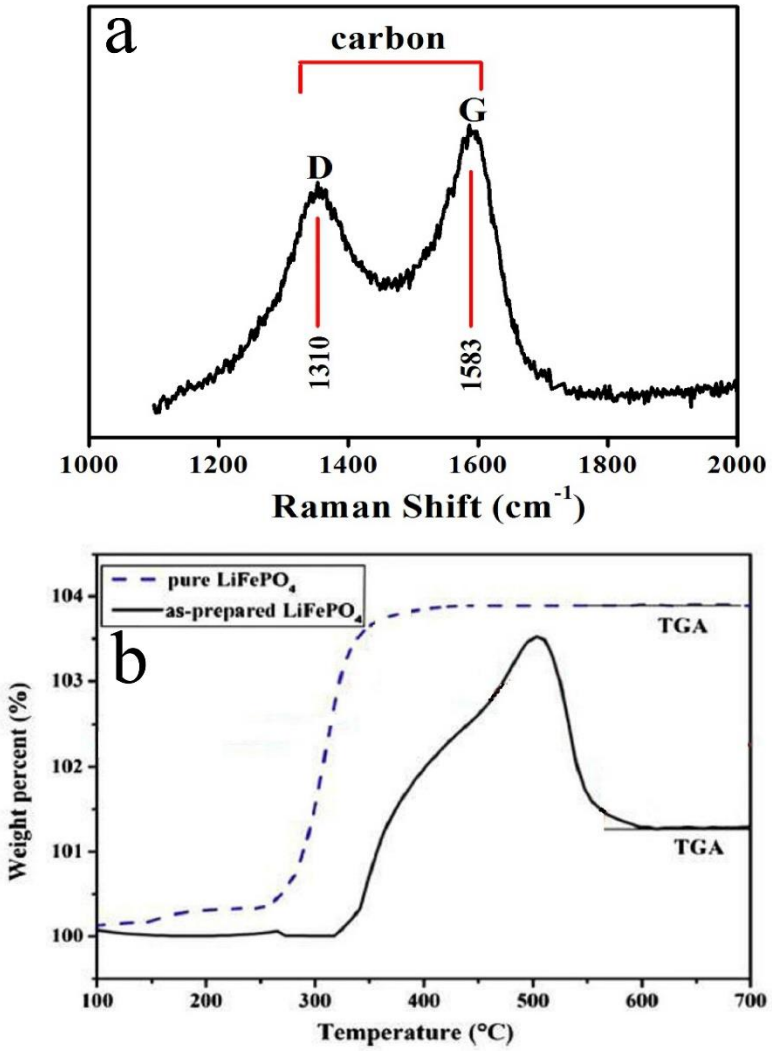

Figure 3. (a) Raman spectrum of the as-prepared hollow $LiFePO_4$/C; (b) the TGA curve of pure $LiFePO_4$ and the as-prepared hollow $LiFePO_4$/C.

Raman spectroscopy was applied to analyze the phase constitution of the hollow $LiFePO_4$/C (Fig. 3a). Two intense broad peaks located at 1310 cm^{-1} and 1583 cm^{-1} are attributed to the D-band (K-point phonos of A_{1g} symmetry) and G-band (E_{2g} phonons of C sp^2 atoms) of graphene, respectively, which indicate that carbon was successfully coated on the surface of the $LiFePO_4$ microspheres.[29, 30] It is believed that the coated carbon should be derived from the citric acid.[31] Thermogravimetric (TG) measurement was used to estimate the carbon content in the hollow $LiFePO_4$/C. As shown in Fig. 3b, in the temperature range of 250-500 ºC, there is a the theoretical weight gain of 5.07 wt%, which is ascribed to the oxidation of olive $LiFePO_4$ to $Li_3Fe_2(PO_4)_3$ and Fe_2O_3.[32] As for the hollow $LiFePO_4$/C, when heated above 350 ºC, the carbon starts to be oxidized to CO_2 gas. After 550 ºC, no obvious mass loss is observed, indicating the carbon was completely removed. It can be calculated that the carbon content in the hollow $LiFePO_4$/C is calculated to be about 2.6 wt%.

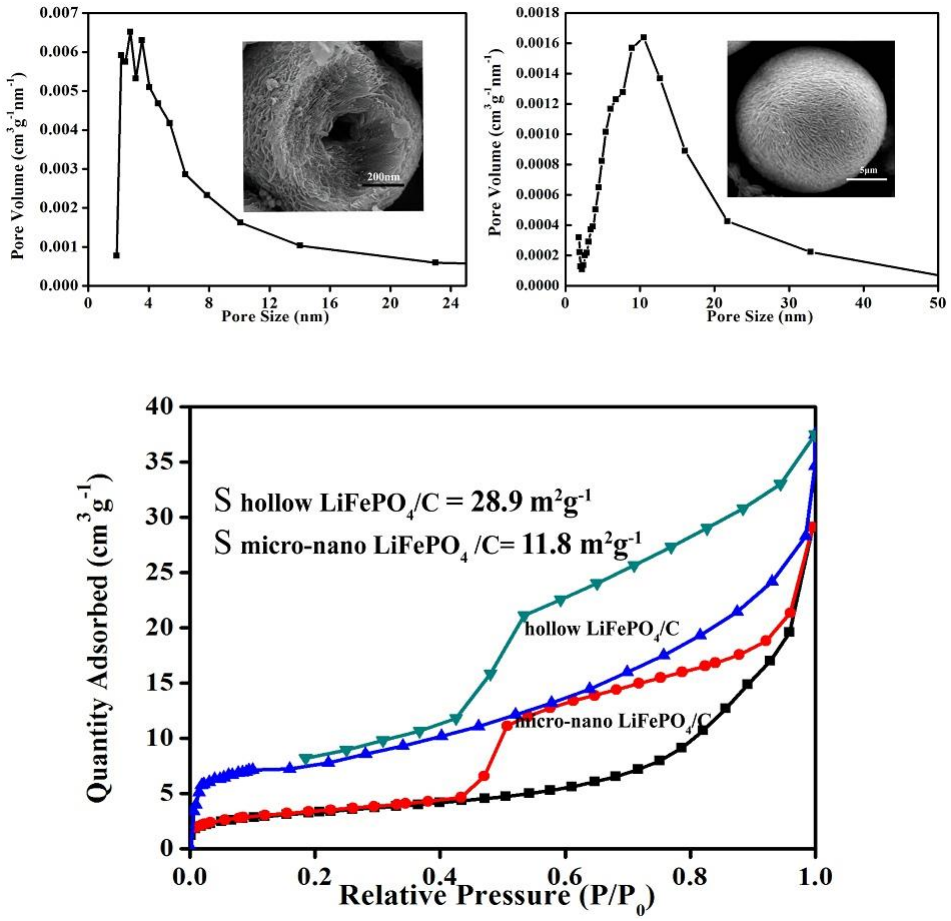

Figure 4. The-BJH pore size distribution curves and specific surface area of the hollow $LiFePO_4/C$ and the micro-nano $LiFePO_4/C$

As shown in Fig. 4, the adsorption isotherm of hollow $LiFePO_4/C$ reveals a type-IV curve with an H3-type hysteresis loop, demonstating a mesoporous characteristic.[17, 20] A wide range of the pore-size distribution from 2 to 100 nm is observed, and most pores are distributed within the range of 2-10 nm. The pore size distribution of the hollow $LiFePO_4/C$ focus on two major peaks which indicates that the distribution of the particle granularity is heterogeneous, however, the pore size distribution of the micro-nano $LiFePO_4/C$ is more concentrated which indicates that the distribution of the particle granularity is very uniform. The experiment result is also in good agreement with the SEM images. It is clear to see that the pore volume of the hollow $LiFePO_4/C$ is much larger than that of the micro-nano $LiFePO_4$. The BET of the hollow $LiFePO_4$ is 28.9 m^2 g^{-1} and that of the micronano $LiFePO_4$ is only 11.8 m^2 g^{-1}, which means that the former could afford abundant interspace for the contact of electrolyte and greatly lower the diffusion distance for Li ion, leading to the higher reversible capacity and rate performance.[32] Additionally, the hollow channel throughout the microstructures could effectively buffer the volume variation of the electrode and possible collapse of the structure during the cycling. Furthermore, the structural stability may also significantly depend on the nature of porosity, pore size distribution, and pore morphology.

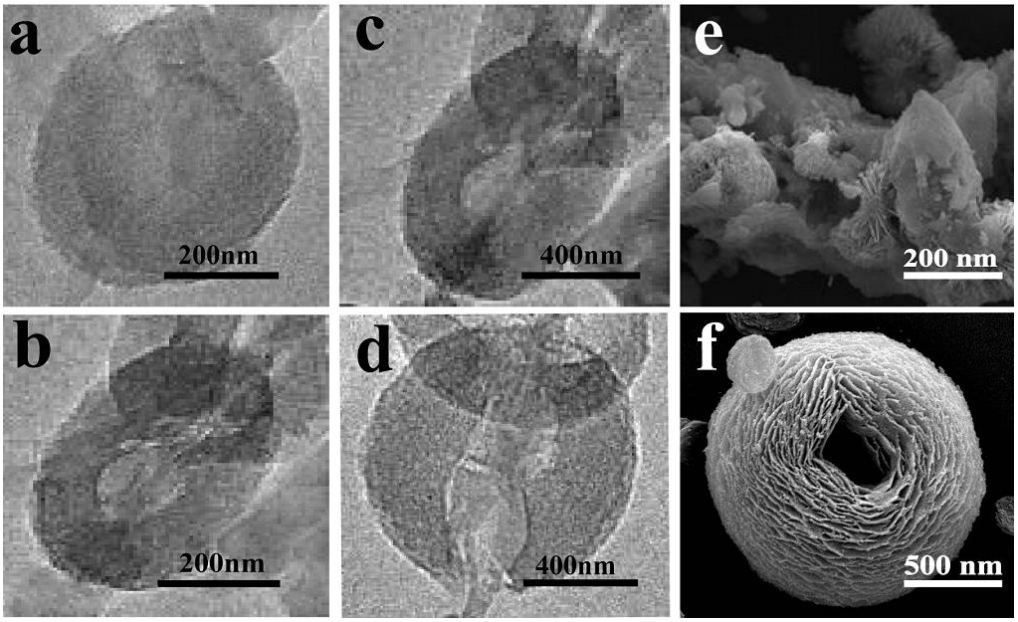

Figure 5. TEM images of samples formed at various time: (a) 2 h, (b) 4 h, (c) 6 h, (d) 8 h; SEM graphics of samples formed at various time: (e) 0.5 h, (f) 8 h;

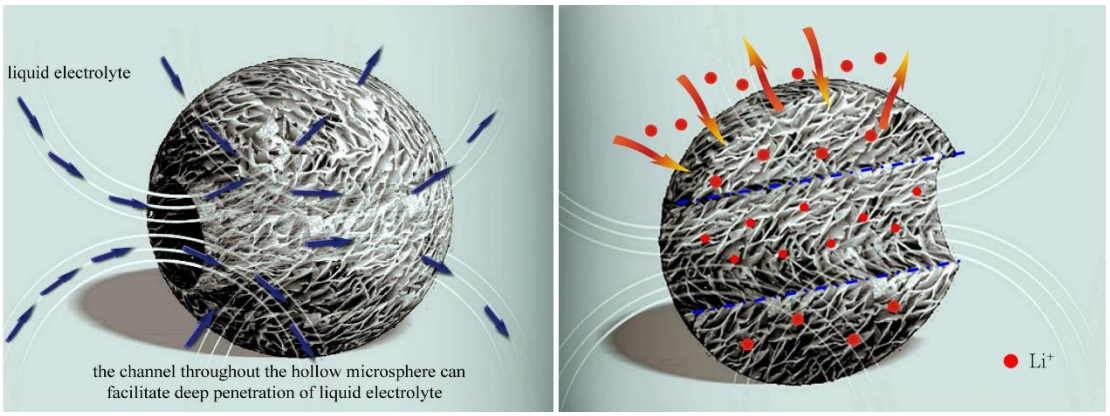

Figure 6. Schematic illustration of the liquid electrolyte deep penetration mechanism in the hollow $LiFePO_4/C$

To investigate the formation mechanism of the hollow $LiFePO_4/C$, intermediate samples formed in different reaction times are investigated by TEM and SEM. As shown in Fig. 5(a-d), the sample in the first 2 h consists of round-likely particles. When the reaction time is extended, the hollow interior appears gradually in the microsphere. Interestingly, the sample after 8h shows an open channel throughout the microsphere. Fig. 5(e, f) shows that the product is composed of nanosheets initially. As reaction time is prolonged, the saddle-shaped morphology gradually transformed to round-like sphere.[22, 33] In the first stage, with the crystal nuclei aggregated, the original particle aggregated and the incompact structure formed. In the following, Ostwald ripening is the dominating formation mechanism.[33]

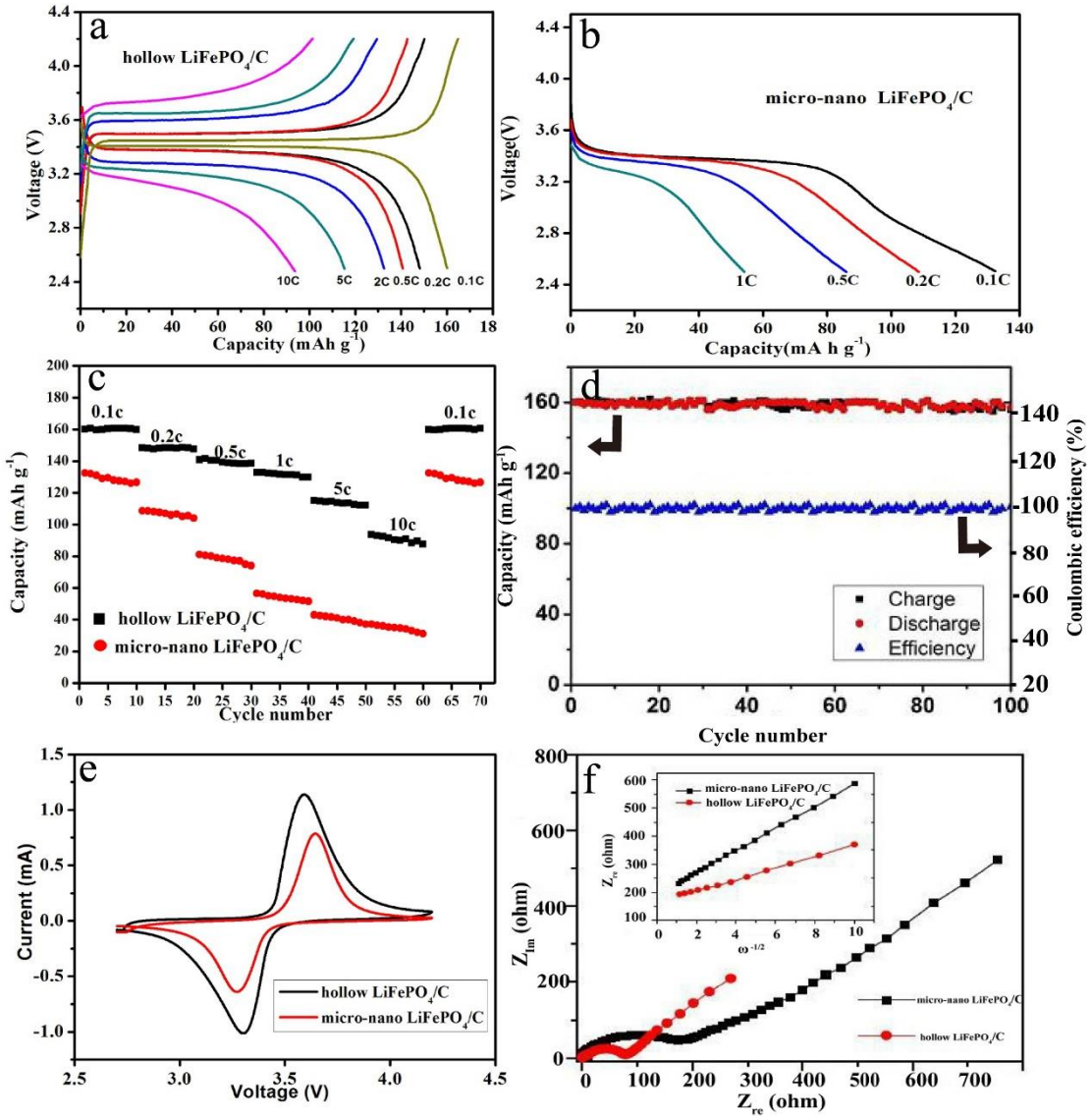

Figure 7. (a) Charge and discharge curves of the hollow $LiFePO_4/C$ at different rates; (b) Discharge curves at different rates for the micro-nano $LiFePO_4/C$; (c) Discharge capacities of the hollow $LiFePO_4/C$ and micro-nano $LiFePO_4/C$ at different rates; (d) Cycle performance and coulombic efficiency profiles of hollow $LiFePO_4/C$ at 0.1 C; (e) Cyclic voltammogram (CV) of the hollow $LiFePO_4/C$ and micro-nano $LiFePO_4/C$ at scan rate 0.1mV s^{-1}; (f) Electrochemical impedance spectroscopy results (EIS) of the hollow $LiFePO_4/C$ and micro-nano $LiFePO_4/C$ (Inset: liner fitting of Warburg impedance).

Fig. 6 shows the schematic illustration of the liquid electrolyte penetrating deeply into the microsphere through the channel. The hollow structure could efficiently improve the invasion of the electrolyte into the material, increase the reaction activity sites, and shorten the Li^+ diffusion way inside the crystal. This unique structure could also facilitate the improvement of cycling stability since its abundant pore structure can ease the volume expansion during the cycling.

The electrochemical performance of the prepared hollow $LiFePO_4/C$ was evaluated by half coin cells in the voltage window of 2.5-4.2 V. For comparison, the micro-nano $LiFePO_4/C$ was also examined. Fig. 7a-b show the charge/discharge curves at different discharge rates from 0.1 C to 10 C. As can be seen, the reversible discharge capacities of hollow $LiFePO_4/C$ are 160, 148, 141, 132.5, 115,

93.5 mAh g^{-1} at current rates of 0.1, 0.2, 0.5, 1, 5, 10 C, respectively. However, those of the micro-nano $LiFePO_4$/C are much lower, 132.5, 108.6, 81.0 and 56.5 mAh g^{-1} at 0.1, 0.2, 0.5 and 1 C, respectively.

Table 1. Comparison between the specific capacities of the hollow $LiFePO_4$/C with those in the literature.

Morphology	**Specific capacity at 0.1, 1, 10 C (**mAh g^{-1}**)**	**Ref**
multiaperture $LiFePO_4$/C microspheres	146, 118 and 90	[34]
polyporous $LiFePO_4$/C microspherical composites	139, 106 and 54	[35]
mesoporous $LiFePO_4$/CNT microspheres	150, 129 and 70	[36]
hollow $LiFePO_4$/C	160,132.5 and 93.5	**This work**

Apparently, the reversible capacity of the hollow $LiFePO_4$/C is highly improved and the polarization at higher rates is greatly reduced compared to the micro-nano $LiFePO_4$/C, which was attributed to the markedly improved active sites for lithium storage and the reduced diffusion distance of Li^+. Fig. 7c shows that the capacity difference between the micro-nano $LiFePO_4$/C and the hollow $LiFePO_4$/C is remarkable even at a high rate of 10 C. These results reveal that obviously enhancement effects on the rate capacity of the hollow $LiFePO_4$/C, in particular for the high rate performance. The specific capacity and rate capacity of the hollow $LiFePO_4$/C is also superior to the earlier mentioned $LiFePO_4$/C materials, more details of the comparison are shown in Table 1.[17, 34-36] These results reveal that the nanosheets assembled microspheres with open hollow channel show a great advantage for improving rate performance of $LiFePO_4$ sample. Fig. 7d shows the cycling stability of the hollow $LiFePO_4$/C at 0.1 C. The as-prepared sample exhibits an excellent cycling stability with no capacity attenuation in the first 100 cycles, which is ascribed to the characteristic 3D hierarchical hollow structures.

Fig. 7e gives the cyclic voltammetry curves of two samples at a scan rate of 0.1 mV s^{-1}. As seen, both samples have a couple of well-defined peaks, consistent with the charge/discharge reaction of the Fe^{3+}/Fe^{2+} redox couple.[37] For comparison, the hollow $LiFePO_4$/C exhibits higher redox peak current density and much less potential gap, revealing much faster Li ion diffusion in the sample.

Fig. 7f compares their EIS curves. The high-frequency intercept of the semicircle is assigned to the uncompensated resistance (R_u) and the diameter of the semicircle refers to the charge-transfer resistance (R_{ct}). R_u includes the particle-particle contact resistance, electrolyte resistance, and the

resistance between the electrode and the current collector. [38, 39] It is observed that the charge-transfer resistance decreases from ~180 Ω in micro-nano $LiFePO_4$ to ~80 Ω in the hollow $LiFePO_4$/C microsphere. The Li-ion diffusion coefficient (D) can also be calculated by the following equation [39, 40]:

$$D = R^2T^2/2A^2n^4F^4C^2\sigma^2$$

Where D is the diffusion coefficient ($cm^2\ s^{-1}$) and σ is the Warburg factor, which is matched with the Zre. It can be calculated by the following equation [41]:

$$Zre = R_c+R_{ct}+\sigma\omega^{-1/2}$$

From the linear curve fitting (Fig. 7f), the Warburg factor (σ) 40.1 and 20.3 $cm^2\ s^{-1/2}$ are obtained for micro-nano $LiFePO_4$ and the hollow $LiFePO_4$/C, respectively. As calculated, the lithium-ion diffusion coefficient of hollow $LiFePO_4$/C is more than 4 times higher than that of micro-nano $LiFePO_4$. These results show that the hollow $LiFePO_4$/C composite presents smaller charge transfer resistance and higher lithium diffusion ability, which are beneficial to the rapid charge and discharge.[34] Such improvements should be due to the significant improvement of lithium insertion kinetics.

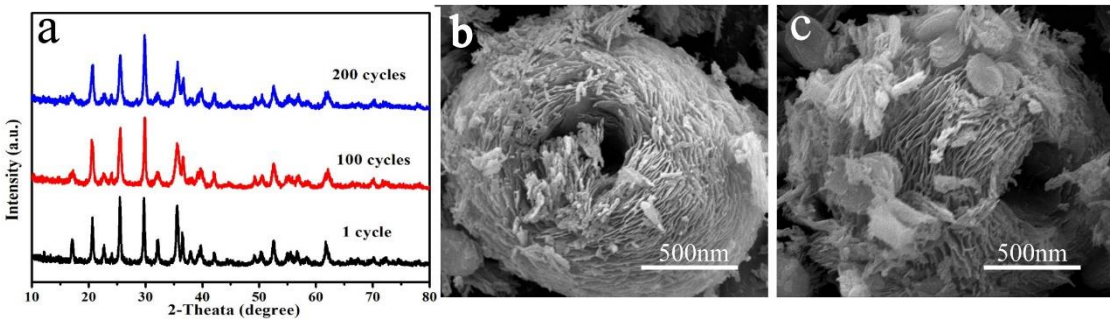

Figure 8. XRD patterns of the hollow $LiFePO_4$/C electrodes after different cycles at 340 mA g^{-1}. Before disassembling, each cell was charged to 3.4 V and then kept at that voltage for 2 h; SEM images of the hollow $LiFePO_4$/C electrode after (b), 100 cycles (c), 200 cycles at 340 mA g^{-1}.

Continuous structure deterioration, electrode slice pulverization, and detachment of active material during the repetitive volume expansion/shrinkage during the Li-ion insertion/extraction are identified as major causes for capacity fading in long-term cycling. The formation of new microstructure was also regarded as good way to guarantee better anti-oxidation and anti-pulverization by Chen and his co-workers.[42-46] Therefore, the structures and surface morphology evolution of the hollow $LiFePO_4$/C after different cycles (1,100, 200) were examined by XRD and SEM (Fig. 8). The main diffraction peaks of electrodes after 100 cycles are almost the same and no new impurity peaks for the electrodes appear, implying excellent structural stability of the hollow $LiFePO_4$/C during the cycling. The SEM images of the cycled sample after 100 and 200 cycles at 340 mA g^{-1} indicate that the hollow microsphere was well maintained during the cycling.

4. CONCLUSIONS

In summary, nanosheets assembled $LiFePO_4$/C with open hollow channel are successfully synthesized by the one-pot template-free hydrothermal method. Interestingly, good balance of high tap density and superior lithium storage performance was achieved for the as-prepared hollow $LiFePO_4$/C. This unique morphology exhibited much higher surface area and provided shorter ion diffusion path. Specially, the channel throughout the hollow microsphere should be in favor of the electrolyte penetration into the inner $LiFePO_4$ and rapid Li-ion transport at the electrode/electrolyte interface. Also, the hollow structure could efficiently reduce the volume change during the charge/discharge process, leading to excellent cycling stability. The as-prepared hollow $LiFePO_4$/C with open channel here could exert potential application as cathode material in lithium ion batteries.

ACKNOWLEDGEMENT
This work was supported by the National Natural Science Foundation of China (Grant No.21276286 and No. 21571189), Hunan Provincial Science and Technology Plan Project of China (2016TP1007 and 2017TP1001) and Hunan Provincial Key Laboratory of Chemical Power Sources.

References

1. M.H. Sun, S.Z. Huang, L.H. Chen, Y. Li, X.Y. Yang, Z.Y. Yuan, B.L. Su, *Chem. Soc. Rev.*, 45 (2016) 347.
2. W.G. Bae, H.N. Kim, D. Kim, S.H. Park, H.E. Jeong, K.Y. Suh, *Adv. Mat.*, 26 (2014) 675.
3. D. Bradshaw, S. El-Hankari, L. Lupica-Spagnolo, *Chem. Soc. Rev.*, 43 (2014) 5431.
4. X.Y. Yang, A. Leonard, A. Lemaire, G. Tian, B.L. Su, *Chem. Commun.*, 47 (2011) 2763.
5. X.J. Meng, F. Nawaz, F.S. Xiao, *Nano. Today*, 4 (2009) 292.
6. N.D. Petkovich, A. Stein, *Chem. Soc. Rev.*, 42 (2013) 3721.
7. B.M. Weckhuysen, J.H. Yu, *Chem. Soc. Rev.*, 44 (2015) 7022.
8. L.H. Chen, X.Y. Li, J.C. Rooke, Y.H. Zhang, X.Y. Yang, Y. Tang, F.S. Xiao, B.L. Su, *J. Mater. Chem.*, 22 (2012) 17381.
9. J. Perez-Ramirez, C.H. Christensen, K. Egeblad, C.H. Christensen, J.C. Groen, *Chem. Soc. Rev.*, 37 (2008) 2530.
10. Z.Y. Yuan, B.L. Su, *J. Mater. Chem.*, 16 (2006) 663.
11. A. Munoz-Bonilla, M. Fernandez-Garcia, J. Rodriguez-Hernandez, *Prog. Polym. Sci.*, 39 (2014) 510.
12. A. Raza, J.Q. Wang, S. Yang, Y. Si, B. Ding, *Carbon Lett.*, 15 (2014) 1.
13. S. Dutta, A. Bhaumik, K.C.W. Wu, *Energ. Environ. Sci.*, 7 (2014) 3574.
14. Y. Li, Z.Y. Fu, B.L. Su, *Adv. Funct. Mater.*, 22 (2012) 4634.
15. T.M. Davis, T.O. Drews, H. Ramanan, C. He, J.S. Dong, H. Schnablegger, M.A. Katsoulakis, E. Kokkoli, A.V. McCormick, R.L. Penn, M. Tsapatsis, *Nat. Mater.*, 5 (2006) 400.
16. B. Angelov, A. Angelova, B. Papahadjopoulos-Sternberg, S. Lesieur, J.F. Sadoc, M. Ollivon, P. Couvreur, *J. Am. Chem. Soc.*, 128 (2006) 5813.
17. Y. Jin, X.C. Tang, H.Y. Wang, *Rsc. Adv.*, 6 (2016) 75602.
18. M. Wang, G.D. Li, H.Y. Xu, Y.T. Qian, J. Yang, *Acs. Appl. Mater. Inter.*, 5 (2013) 1003.
19. X.Y. Lai, J.E. Halpert, D. Wang, *Energ. Environ. Sci.*, 5 (2012) 9944.
20. C.W. Sun, S. Rajasekhara, J.B. Goodenough, F. Zhou, *J. Am. Chem. Soc.*, 133 (2011) 2132.

21. Y.L. Ruan, Z.Y. Tang, *Acta. Chim. Sinica*, 66 (2008) 680.
22. S.Y. Gao, S.X. Yang, J. Shu, S.X. Zhang, Z.D. Li, K. Jiang, *J.Phys.Chem.C.*, 112 (2008) 19324.
23. Y. Jin, X. Tang, H. Wang, *Rsc. Adv.*, 6 (2016) 75602.
24. S.W. Oh, S.T. Myung, S.M. Oh, K.H. Oh, K. Amine, B. Scrosati, Y.K. Sun, *Adv.Mater.*, 22 (2010) 4842.
25. A. Paolella, G. Bertoni, S. Marras, E. Dilena, M. Colombo, M. Prato, A. Riedinger, M. Povia, A. Ansaldo, K. Zaghib, *Nano. Lett.*, 14 (2014) 6828.
26. B. Wang, T. Liu, A. Liu, G. Liu, L. Wang, T. Gao, D. Wang, X.S. Zhao, *Adv. Energy. Mater.*, 6 (2016) 1600426.
27. D. Li, Q. Qin, X.C. Duan, J.Q. Yang, W. Guo, W.J. Zheng, *Acs. Appl. Mater. Inter.*, 5 (2013) 9095.
28. H.J. Kim, K.I. Choi, A.Q. Pan, I.D. Kim, H.R. Kim, K.M. Kim, C.W. Na, G.Z. Cao, J.H. Lee, *J. Mater. Chem.*, 21 (2011) 6549.
29. C.L. Gong, Z.G. Xue, S. Wen, Y.S. Ye, X.L. Xie, *J. Power. Sources*, 318 (2016) 93.
30. X.F. Tu, Y.K. Zhou, X.H. Tian, Y.J. Song, C.J. Deng, H.X. Zhu, *Electrochim. Acta*, 222 (2016) 64.
31. S.H. Ng, J.Z. Wang, D. Wexler, K. Konstantinov, Z.P. Guo, H.K. Liu, *Angew. Chem. Int. Edit*, 45 (2006) 6896.
32. H. Gong, H.R. Xue, T. Wang, J.P. He, *J. Power. Sources*, 318 (2016) 220.
33. B. Liu, H.C. Zeng, *Small*, 1 (2005) 566.
34. R.R. Chen, Y.X. Wu, X.Y. Kong, *J. Power. Sources*, 258 (2014) 246.
35. F. Yu, J.J. Zhang, Y.F. Yang, G.Z. Song, *J. Power. Sources*, 195 (2010) 6873.
36. L.Y. Tan, Q.L. Tang, X.H. Chen, A.P. Hu, W.N. Deng, Y.S. Yang, L.S. Xu, *Electrochim. Acta*, 137 (2014) 344.
37. W.B. Luo, S.L. Chou, Y.C. Zhai, H.K. Liu, *J. Mater. Chem. A.*, 2 (2014) 4927.
38. G.B. Zeng, R. Caputo, D. Carriazo, L. Luo, M. Niederberger, *Chem. Mater.*, 25 (2013) 3399.
39. Y. Zhao, L.L. Peng, B.R. Liu, G.H. Yu, *Nano. Lett.*, 14 (2014) 2849.
40. J. Mosa, M. Aparicio, A. Duran, C. Laberty-Robert, C. Sanchez, *J. Mater. Chem. A.*, 2 (2014) 3038.
41. Y. Gao, Q. Zhao, Z.H. Xu, Y.G. Sun, *New. J. Chem.*, 38 (2014) 2629.
42. J. Park, W.A. Appiah, S. Byun, D. Jin, M.H. Ryou, Y.M. Lee, *J. Power. Sources*, 365 (2017) 257.
43. S. El Khakani, J.C. Forgie, D.D. MacNeil, D. Rochefort, *J. Electrochem. Soc.*, 162 (2015) A1432.
44. J.Y. Luo, Y.Y. Xia, *Adv. Funct. Mater.*, 17 (2007) 3877.
45. H.T. Sun, G.Q. Xin, T. Hu, M.P. Yu, D.L. Shao, X. Sun, J. Lian, *Nat. Commun.*, 5 (2014) 23.
46. A. Caballero, J. Morales, O.A. Vargas, *J. Power. Sources*, 195 (2010) 4318.